IGA of a Photocathode

1 Geometry

The current geometry was derived from the technical drawings in [1]. Some simplifications were made especially regarding the inner part of the electrode, such that the geometry can be modeled as being rotationally symmetric. The relative permittivity of the insulator was retrieved from a CST model to be 9.4. The geometry is depicted in fig. 1. The numbers refer to the individual patches in the context of IGA. The patch boundaries are indicated by the black lines. The red lines represent homogeneous Dirichlet boundary conditions, the blue lines inhomogeneous Dirichlet boundary conditions with a value of -60kV and the green lines indicate homogeneous Neumann boundaries. According to the technical drawings patch 10 as well as parts of patches 7 and 8 should consist of insulator material. In the case of patch 10 this is already included in the model and it could also be added in the other cases.

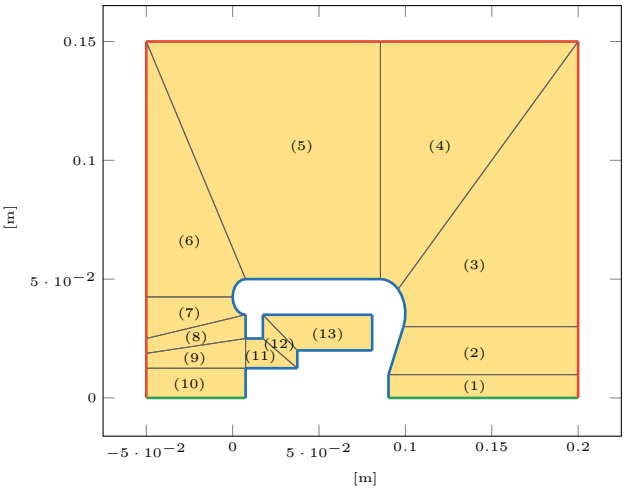

Figure 1: Photocathode geometry and boundary conditions.

2 Electrostatic Potential and Electric Field

The solution for the electrostatic potential is shown in fig. 2. Fig. 3 depicts the absolute value of the electric field. Both of the solutions were computed

with $p = 5$ as the degree of the basis functions and $n_{\text{sub}} = 16$ as the number of elements that each knot vector is uniformly split into. On the boundary of patches 5 and 6 the solution seems to depend on the boundary. Also the sharp corners on the left boundary of patch 11 seem to lead to a similiar behavior. Choosing n_{sub} larger may resolve these issues.

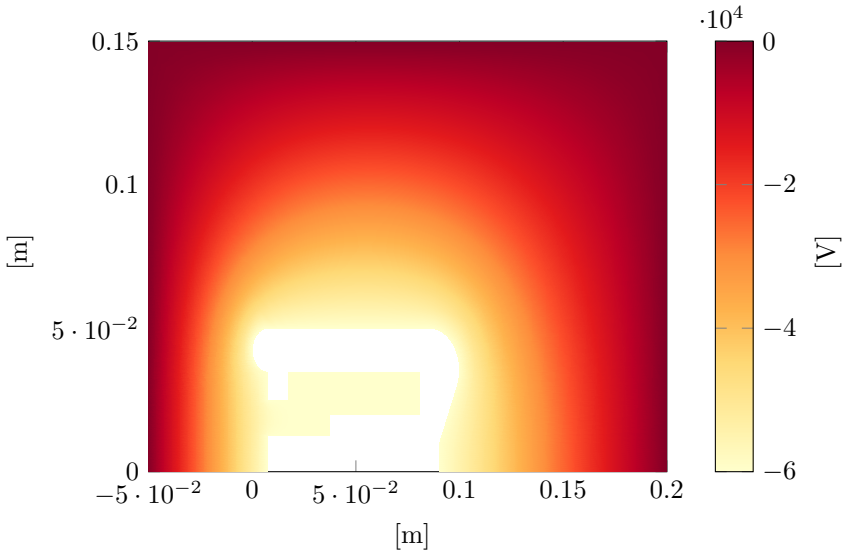

Figure 2: Electrostatic potential.

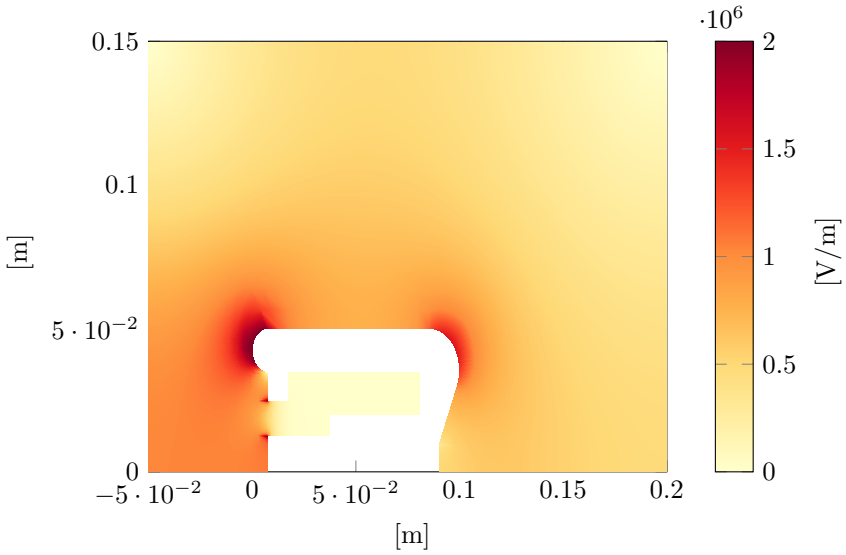

Figure 3: Absolute value of the electric field.

3 Convergence Study

The convergence studies investigate the accuracy of the solution while increasing the number of elements per patch. (Akin to h-refinement in classical FEA) Since no analytic solution exists a reference with $p = 5$ and $n_{\text{sub}} = 16$ was chosen arbitrarily. The relative errors are then computed in respect to this solution.

The errors are computed as

$$e_{L^2} = \frac{\|\varphi_{\text{it}}\|_{L^2} - \|\varphi_{\text{ref}}\|_{L^2}}{\|\varphi_{\text{ref}}\|_{L^2}} \tag{1}$$

and (2)

$$e_{H^1} = \frac{\|\varphi_{\text{it}}\|_{H^1} - \|\varphi_{\text{ref}}\|_{H^1}}{\|\varphi_{\text{ref}}\|_{H^1}} \tag{3}$$

where

$$\|\varphi\|_{H^1} = \|\varphi\|_{L^2} + \|\nabla\varphi\|_{L^2}. \tag{4}$$

The integrals associated with the L^2-norm are evaluated using a quadrature rule defined on each element of a given patch.

The degrees of the basis functions are given in the legend, as well as theoretical limits for the convergence rates. They are given by $p + 1$ in the case of the L^2-norm (electrostatic potential) and p in the case of the H^1-norm (electric field). As seen in fig. 4 and fig. 5 we observe convergence.

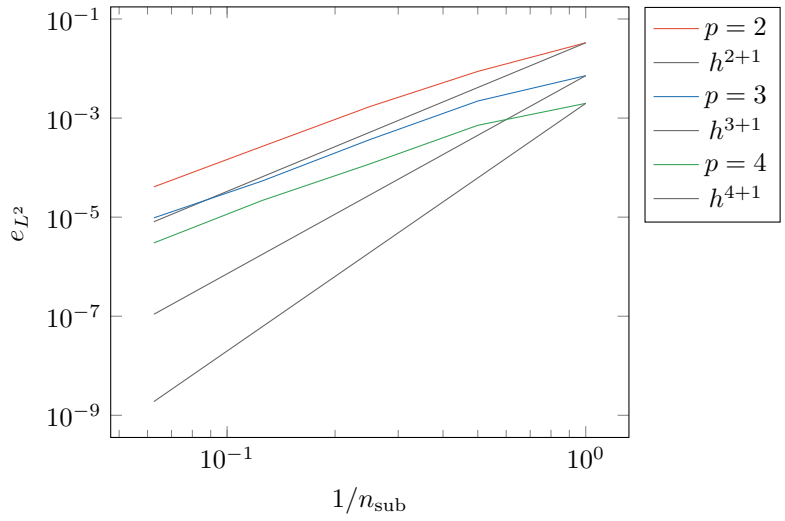

Figure 4: Convergence of L^2-norm.

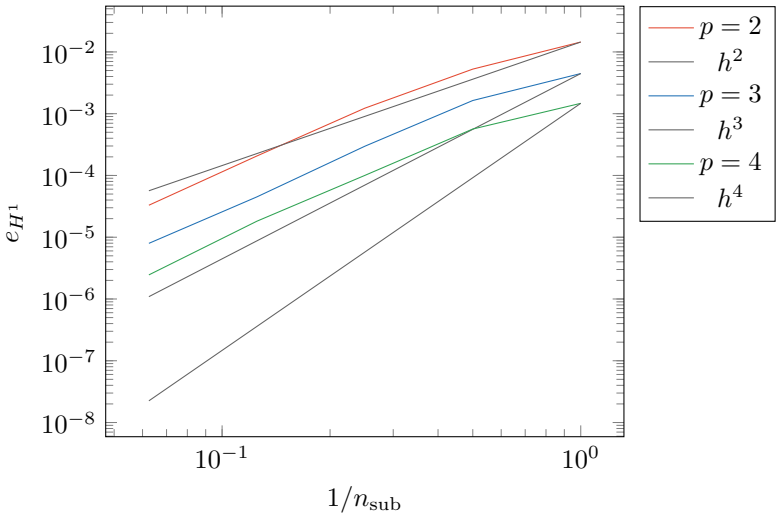

Figure 5: Convergence of H^1-norm.

Lastly the strange behavior observed in sec. 2 was investigated by displaying the error on every individual element of the mesh. In the case of fig. 6 $n_{\text{sub}} = 1$ and $p = 2$ were used and for fig. 7 we chose $n_{\text{sub}} = 16$. The reference remained the same as before for both plots. The figures also indicate convergence for the elements in question, along with giving and idea of the magnitude of the absolute error on these.

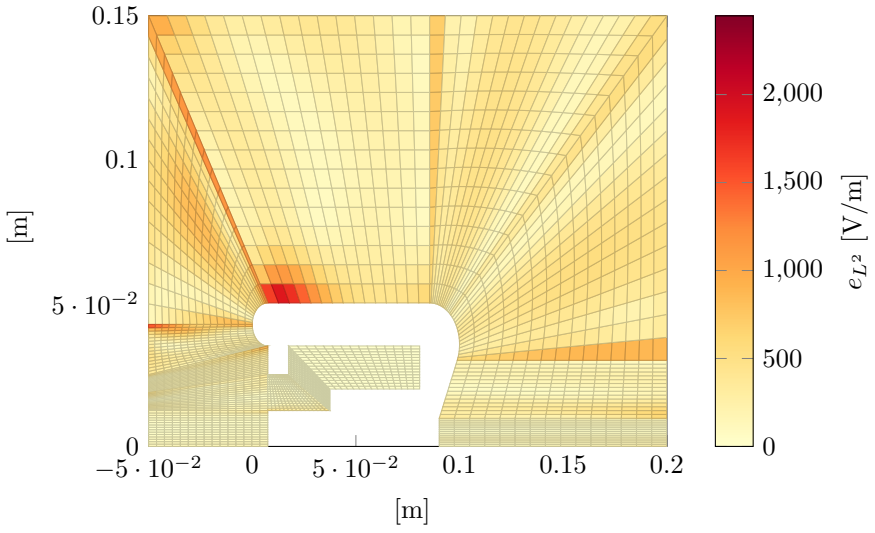

Figure 6: Absolute error of the electric field on every element.

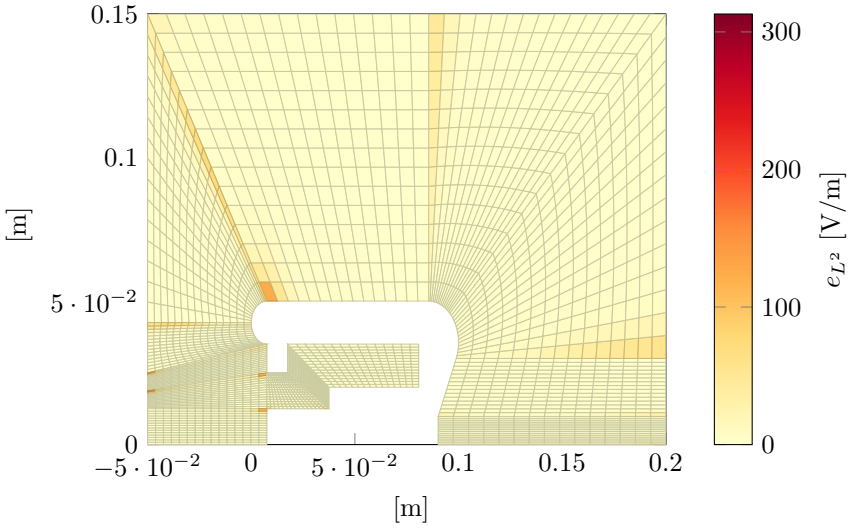

Figure 7: Absolute error of the electric field on every element.

References

[1] Martin Espig. *Development, construction and characterization of a variable repetitive spin-polarized electron gun with an inverted-geometry insulator.* PhD thesis, Technische Universität Darmstadt, 2016.